MOLECULAR IMAGING AND BIOLOGY

Mol Imaging Biol (2019) 21:465–472
DOI: 10.1007/s11307-018-1276-x

Published Online: 7 September 2018

RESEARCH ARTICLE

Ferumoxytol Can Be Used for Quantitative Magnetic Particle Imaging of Transplanted Stem Cells

Hossein Nejadnik,[1] Prachi Pandit,[2] Olga Lenkov,[1] Arian Pourmehdi Lahiji,[1] Ketan Yerneni,[1] Heike E. Daldrup-Link[1,3]

[1]*Pediatric Molecular Imaging Program in the Molecular Imaging Program at Stanford (MIPS), Department of Radiology, Stanford University School of Medicine, 725 Welch Rd, Rm 1665, Stanford, CA, 94305-5654, USA*
[2]*Magnetic Insight Inc, Alameda, CA, USA*
[3]*Department of Pediatrics, Stanford University School of Medicine, Stanford, CA, USA*

Abstract
Purpose: To evaluate, if clinically translatable ferumoxytol nanoparticles can be used for *in vivo* detection and quantification of stem cell transplants with magnetic particle imaging (MPI).
Procedures: Mesenchymal stem cells (MSCs) were labeled with ferumoxytol or ferucarbotran and underwent MPI, magnetic resonance imaging (MRI), Prussian blue staining, and inductively coupled plasma (ICP) spectrometry. Unlabeled, ferumoxytol, and ferucarbotran-labeled MSCs were implanted in calvarial defects of eight mice and underwent MPI, MRI, and histopathology. The iron concentration calculated according to the MPI signal intensity and T2 relaxation times of the three different groups were compared using an analysis of variance (ANOVA) with Bonferroni correction, and a $p < 0.05$.
Results: Compared to unlabeled controls, ferumoxytol- and ferucarbotran-labeled MSC showed significantly increased iron content, MPI signal and MRI signal. The ferumoxytol MPI signal was approximately 4× weaker compared to ferucarbotran at equimolar concentrations ($p = 0.0003$) and approximately 1.5× weaker for labeled cells when using optimized labeling protocols ($p = 0.002$). *In vivo*, the MPI signal of ferumoxytol-labeled MSC decreased significantly between day 1 and day 14 ($p = 0.0124$). This was confirmed by histopathology where we observed a decrease in Prussian blue stain of MSCs at the transplant site. The MRI signal of the same transplants did not change significantly during this observation period ($p = 0.93$).
Conclusion: Ferumoxytol nanoparticles can be used for *in vivo* detection of stem cell transplants with MPI and provide quantitative information not attainable with MRI.

Key Words: Stem cell, MRI, MPI, Molecular imaging

Introduction

Complex bone injuries due to osteoarthritis, trauma, or surgery are debilitating for individuals and require significant medical intervention [1–4]. More than 2 million bone grafts are transplanted each year, representing the second most commonly transplanted materials after blood products and causing health care costs in the order of $21 billion every year [5]. Considering escalating demands, limited availability and limited efficacy of bone allografts, new options for bone repair are urgently needed. Stem cell transplants are attractive alternatives because they are

Correspondence to: Heike Daldrup-Link; *e-mail:* H.E.Daldrup-Link@stanford.edu

immediately available in potentially unlimited quantities, less expensive and represent "live" tissue with potentially better engraftment outcomes [1–4].

However, successful development of stem cell-mediated bone repair is hampered by limited survival and engraftment of locally administered therapeutic cells. Reported engraftment outcomes of locally engrafting stem cells are quite modest [6–8]. Important factors that may cause death of the transplanted cells are a locally hostile environment or graft rejection [9–11]. A non-invasive imaging test, which could accurately monitor and quantify transplanted stem cells over time would substantially advance stem cell based bone regeneration approaches.

Magnetic particle imaging (MPI) is an emerging molecular imaging technique that can non-invasively detect and quantify iron oxide-labeled cells *in vivo* [12, 13]. MPI images detect iron without non-specific background signal and provide exquisite sensitivity and specificity [14]. Though promising, stem cell imaging with MPI has been performed with experimental iron oxide nanoparticles thus far (*e.g.*, ferucarbotran). To enable clinical translation, it would be preferable to label and track therapeutic cells with a clinically applicable iron label. Ferumoxytol is currently FDA approved as an iron supplement for the treatment of anemia in patients with renal insufficiency. Several institutions in North America are using ferumoxytol "off label" for vascular imaging and cancer imaging purposes [15–17]. Ferumoxytol is immediately clinically available for imaging applications in patients through an "off label" use. While initially not detectable with MPI, improvements of the MPI technology recently enabled detection of ferumoxytol nanoparticles *in vitro* [18]. However, it is not known, if MPI is sensitive enough to detect ferumoxytol-labeled stem cells *in vivo*. Therefore, the goal of this study was to evaluate, if ferumoxytol nanoparticles can be used for *in vivo* detection and quantification of stem cell transplants with MPI.

Materials and Methods

Iron Nanoparticles

Ferumoxytol (Feraheme™, AMAG Pharmaceuticals) is an iron oxide nanoparticle compound composed of an iron oxide core and a carboxymethyl-dextran coat [19, 20]. Ferumoxytol is approved by the FDA for the treatment of iron deficiency anemia [21]. Ferumoxytol nanoparticles have a hydrodynamic diameter of 20–30 nm, an r1 relaxivity of 15 mM^{-1} s^{-1} and an r2 relaxivity of 89 mM^{-1} s^{-1} at 1.5 Tesla and 37 °C [22]. Ferumoxytol can be internalized into stem cells using optimized labeling procedures [17, 23].

Ferucarbotran (VivoTrax™, Magnetic Insight Inc., Alameda, CA) is an iron oxide nanoparticle compound composed of an iron oxide core and a carboxydextran coat [24, 25]. Ferucarbotran nanoparticles have a mean hydrodynamic diameter of 62 nm, an r1 relaxivity of 7.2 ± 0.1 mM^{-1} s^{-1}, and an r2 relaxivity of 82.0 ± 6.2 mM^{-1} s^{-1} at 1.5 Tesla and 37 °C [26]. Ferucarbotran has been used extensively for clinical MRI [24, 25], but has been withdrawn from the US clinical market and recently reformulated for pre-clinical MRI and MPI applications [18].

Stem Cell Labeling

Murine mesenchymal stem cells were harvested from the bone marrow of the bilateral femurs and tibias of eight 6 to 8-week-old female C57BL/6J (Jackson Laboratory) mice. The donor mice were euthanized, both femurs and tibias were explanted, both epiphyses removed with a scalpel, a 25-*gauge needle* was inserted into the bone marrow cavity, and a 10-cc *syringe* filled with DMEM/F12 with Glutamax was attached to the needle and used to *flush* the *bone marrow* cells out of the marrow cavity. The collected *marrow cells* were cultured in T75 flasks with MSC medium supplemented with 10 % FBS, 1 % pen-strep, and 50 pg/ml of human fibroblastic growth factor. The medium was changed approximately every 3–5 days, and the cells were distributed to new flasks when they reached confluence. This process removed non-adherent red and white blood cells, and thereby, separated the adherent MSC over time. Twenty-four hours before labeling, cells were detached and re-plated at a confluency of 5 million cells per flask. Then, cells were labeled with either ferumoxytol nanoparticles (Feraheme™, AMAG Pharmaceuticals, Waltham, MA, 100 µg/ml media) using Lipofectin® (Life Technologies) or labeled with ferucarbotran (Magnetic Insight, Inc., Alameda, CA, 50 µg/ml media) as previously described [23].

Cellular Iron Uptake

Twenty-five, 50, 100, 200, and 500×10^3 cells of both ferumoxytol- and ferucarbotran-labeled MSCs were washed three times with phosphate-buffered saline (PBS) (Gibco, Grand Island, NY), mixed with 30 µl of the polyethylene glycol scaffold and moved to 3 mm NMR tubes for further *in vitro* assessments. Iron uptake of labeled cells was visualized *via* Prussian blue staining with the Accustain Iron Stain Kit (Sigma-Aldrich, St. Louis, MO) using a pararosaniline counter stain. Iron uptake was further quantified by inductively coupled plasma optical emission spectrometry (ICP-OES, Optima 5300 DV, Perkin-Elmer, Waltham, MA).

Animal Model Preparation

Animal experiments were approved by the Stanford Administrative Panel on Laboratory Animal Care (APLAC protocol 27,357). All animals were treated as established by the National Research Council's Guide for the Care and Use of Laboratory Animals. All experiments were performed under isoflurane anesthesia, and buprenorphine was given for pain control after surgeries. One million murine bone marrow-derived MSCs were suspended in

scaffolds (50 µl) consisting of polyethylene glycol conjugated to dimethacrylate. Ammonium persulfate and tetramethylethylenediamine (TMEDA) were used to catalyze the polymerization of acrylamide, forming a polyacrylamide gel. A circular window (diameter: 4 mm) was created in the parietal skull bone of eight female C57BL/6J mice under 1.5 % isoflurane inhalation anesthesia. The MSC-seeded scaffolds were implanted into these windows. Three mice received transplants of ferumoxytol-labeled MSCs, three mice received ferucarbotran-labeled MSCs, and two mice receive unlabeled MSCs transplants. All mice underwent MRI and MPI on days 1 and 14 under isoflurane anesthesia (Fig. 1).

Magnetic Particle Imaging

Magnetic particle imaging was performed with the Momentum MPI scanner (Magnetic Insight Inc., Alameda, CA), a projection field-free line (FFL) scanner, operating with a magnetic field gradient strength of 6 × 6 T/m. Samples translated along the *z*-axis of the scanner using a single-axis translation stage, with FFL along *y*-axis and excitation field (45 kHz, 20 mT peak amplitude) along *z*-axis. Images were reconstructed using *x*-space MPI reconstruction algorithm [27].

For nanoparticle characterization, tracer stock solutions were serially diluted with deionized water, and 1 µl point source phantoms were prepared with tracer concentrations of 100 %, 50 %, 20 %, 10 %, 5 %, and 2 %. For ferumoxytol (stock concentration of 30 µg/µl Fe), this ranged from 30 to 0.6 µg of Fe in PBS, while for ferucarbotran (VivoTrax™ stock concentration of 5.5 µg/µl Fe) this ranged from 5.5 to 0.11 µg of Fe in PBS. Samples were prepared and imaged in triplicate for both tracers using 2D coronal projection images with a field of view (FOV) of 6 cm × 10 cm and acquisition time of 10 s per projection.

In vitro samples were prepared in duplicates and 2D coronal projection images with a FOV of 6 cm × 10 cm and acquisition time of 10 s per projection were acquired for both contrast agent groups and each of the duplicate test tubes, containing 25, 50, 100, 200, and 500×10^3 labeled cells in 30 µl of the agarose scaffold.

For the *in vivo* experiments, 2D coronal projection images with a FOV of 6 cm × 10 cm were first acquired for localization. This was followed by 3D tomographic images with 55 projections with total imaging time of 40 mins, including reconstruction. A FOV of 6 cm × 6 cm × 6 cm was imaged to include the mouse head with the implant, as well as a set of three fiducials with known tracer concentration (10 %, 5 %, 5 % in 1 µl volume) for quantification purposes.

Data analysis was performed with the VivoQuant software (inviCRO, Boston, MA). For tracer characterization, regions of interest (ROIs) were drawn around detectable signal in the MPI images and a linear regression model from the MPI signal at each concentration was used to assess the signal linearity. Tracer resolution was estimated using the measured full-width, half-maximum (FWHM) generated by a single-point source of signal. A calibration curve for iron content to MPI sum signal in the whole ROI was established for both contrast agents, and subsequently used

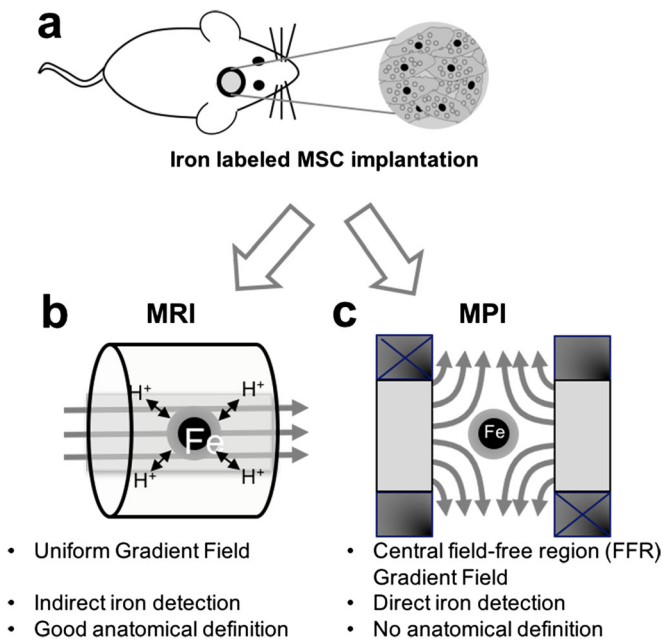

Fig. 1. Principle of iron oxide nanoparticle detection with MPI and MRI. **a** nanoparticle-labeled therapeutic cells, implanted in calvarial defects of a mouse. **b** MRI can depict the cell transplant within the surrounding anatomy. The iron label is detected indirectly, based on alterations of proton T1 and T2 relaxation times. **c** MPI can directly detect and quantify the iron within labeled stem cells.

to quantify the iron content in the *in vitro* cell samples. For *in vivo* quantification, volumetric ROIs were defined over the cell scaffold as well as the fiducials. Iron content and number of implanted cells in the scaffolds were evaluated from a regression model based on the MPI sum signal from the three fiducials with known iron content.

Magnetic Resonance Imaging

All mice with stem cell implants were scanned with a 7T MR scanner (Discovery MR901; collaboration between Agilent [Santa Clara, Calif] and Bruker) using a 2-cm inner diameter mouse head RF coil (Bruker Biospin, Billerica, MA). T2 relaxation times were measured using multi-echo spin echo (MESE) sequences with a repetition time of 2000 ms and multiple echo times (TE) of 6, 13, 20, 27, 34, and 41 ms. All images were obtained using a field of view (FOV) of 25 × 25 mm, a 256 × 256 matrix, 0.5 mm slice thickness, and two acquisitions. T2 relaxation times were calculated by using the Paravision software (Bruker Biospin, Billerica, MA). After the last MRI scans, mice were sacrificed, and stem cell implants were explanted, fixed, paraffin embedded, and cut into 7-µm slices for histological processing. For iron nanoparticle staining, DAB-Prussian blue with the Accustain Iron Stain kit (Sigma-Aldrich, St. Louis, MO) and a Pararosaniline solution counterstain was used. The number of labeled cells were quantified under the microscope in five random high power fields (× 40) and compared between day 1 and 14.

Statistical Analysis T2 relaxation times, ICP results, and estimated iron concentrations based on the MPI signal were compared between ferumoxytol-labeled cells, ferucarbotran-labeled cells, and unlabeled controls (*in vitro*) or ferumoxytol- and ferucarbotran-labeled cell transplants (-*in vivo*), using an analysis of variance (ANOVA) and a $p < 0.05$. A Bonferroni correction was applied for statistical comparisons of *in vitro* data.

Results

Magnetic Particle Imaging of Ferumoxytol Nanoparticles

First, we evaluated the sensitivity of MPI to detect ferumoxytol nanoparticles in solution by evaluating MPI images of cell samples that were labeled with increasing concentrations of ferumoxytol and ferucarbotran. Ferumoxytol resulted in a blooming effect of the MPI signal, which expanded beyond the test tube, over an area of 5 mm^3. The ferumoxytol MPI signal showed a linear correlation with the ferumoxytol concentration (Fig. 2, $R^2 > 0.99$). The minimum detectable ferumoxytol concentration was 1 % (0.3 µg/µl Fe) in a 1-µl volume. By comparison, ferucarbotran showed approximately four times stronger MPI signal at equivalent concentrations (Fig. 2b) and a narrower signal spread compared to ferumoxytol (Fig. 2). Using the FWHM measurement from the point

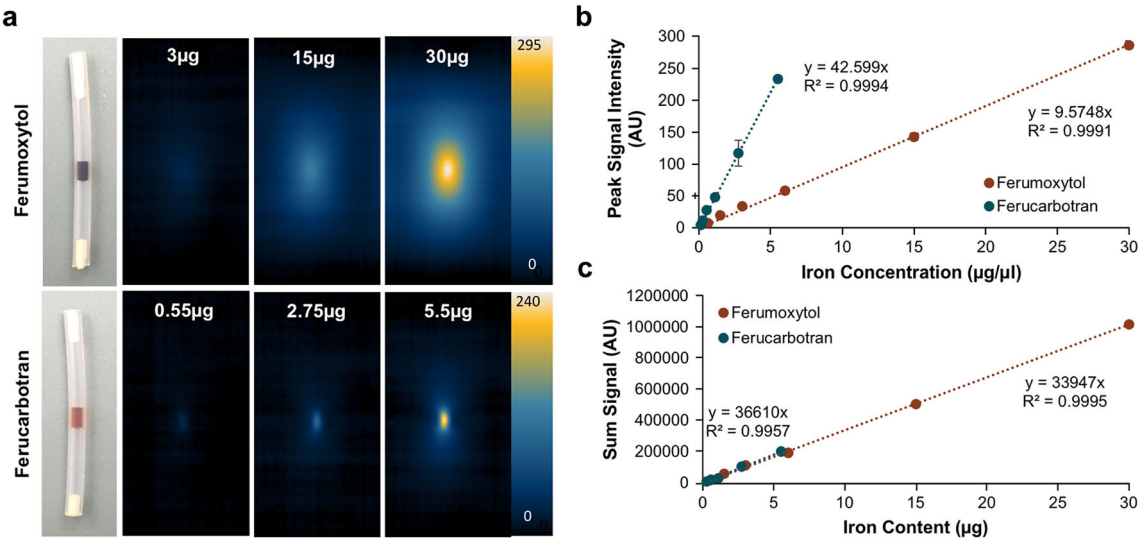

Fig. 2. MPI signal of ferumoxytol and ferucarbotran containing test tubes. **a** MPI images of test tubes with increasing concentrations of ferumoxytol and ferucarbotran in 1 µl of phosphate-buffered saline (PBS, 1 $µm^3$). Ferumoxytol nanoparticles showed a blooming effect with an MPI signal that expanded beyond the test tube, over an area of 5 mm^3. By comparison, ferucarbotran nanoparticles showed less blooming effect with a signal spread over an area of 1 mm^3. **b** Linear correlation between peak MPI signal and Fe concentration for both ferumoxytol and ferucarbotran. The slope for ferucarbotran is higher than ferumoxytol, indicating higher sensitivity of the MPI technique to detect ferucarbotran compared to ferumoxytol. For equivalent iron concentrations, ferucarbotran displays a higher peak signal intensity as compared to ferumoxytol. **c** Calibration curve for total iron content to MPI sum signal for both nanoparticle compounds.

source signal, the resolution for ferumoxytol is ~5 mm, compared ~1 mm for ferucarbotran.

In Vitro Imaging of Ferumoxytol-Labeled MSCs

Magnetic Particle Imaging

Next, we evaluated the sensitivity of MPI to detect ferumoxytol-labeled MSC. The calibration curve from Fig. 2c was used to calculate the total iron content in each cell sample. The MPI signal and correspondingly the total iron content in ferumoxytol-labeled MSC (2.11 ± 0.12 µg of Fe in 500 K cells) was significantly higher compared to unlabeled cells (0.0005 ± 0.002 µg of Fe in 500 K cells) and varied linearly with the number of labeled cells ($R^2 > 0.98$). When using optimized labeling protocol for either tracers, the MPI signal of ferumoxytol-labeled cells was approximately 1.5× weaker compared to ferucarbotran-labeled cells ($p = 0.002$) (Fig. 3b).

The iron uptake per cell was calculated to be 4.656 ± 0.46 pg/cell for ferumoxytol-labeled MSC (100 µg/ml), 6.267 ± 0.61 pg/cell for ferucarbotran-labeled MSC (50 µg/ml), and 0.001 ± 0.00 pg/cell, $p = 0.0001$ for unlabeled cells.

Histopathology and ICP

Ferumoxytol and ferucarbotran were efficiently internalized into MSCs, as confirmed by Prussian blue staining and ICP results (Fig. 4). Prussian blue stains demonstrated marked iron uptake within MSCs labeled with ferumoxytol and ferucarbotran (Fig. 4a). The quantitative iron uptake, as determined by ICP-OES, for MSCs labeled with 100 µg/mL ferumoxytol and 50 µg/ml ferucarbotran and was 4.01 pg/cell ± 0.18 and 4.58 pg/cell ± 0.50 respectively, which did not show a significant difference ($p = 0.14$).

In vivo Imaging of Labeled MSC Implants

Magnetic Particle Imaging

Finally, we investigated the ability of MPI to detect and quantify transplanted stem cells *in vivo* at day 1 and day 14 after transplantation of ferumoxytol-labeled, ferucarbotran-labeled, and unlabeled MSC in calvarial defects. As seen in Fig. 5, ferumoxytol-labeled MSC implants showed significantly higher MPI signal and correspondingly higher calculated Fe content compared to unlabeled MSC implants ($p = 0.0005$) and significantly lower calculated Fe content compared to ferucarbotran-labeled MSC implants ($p = 0.0018$). The MPI signal decreased significantly between day 1 and 14 for both ferumoxytol- and ferucarbotran-labeled MSC ($p = 0.0124$, $p = 0.0001$). This corresponds to a decreased DAB-Prussian blue stain in the transplant site on histology (Fig. 5e–f).

Magnetic Resonance Imaging

T2 relaxation times of ferucarbotran-labeled MSCs (4.16 ± 0.40 ms) and ferumoxytol-labeled MSCs (4.58 ± 0.04 ms) were significantly shorter than those of unlabeled MSCs (26.3 ± 0.5 ms). The mean T2 relaxation time did not change

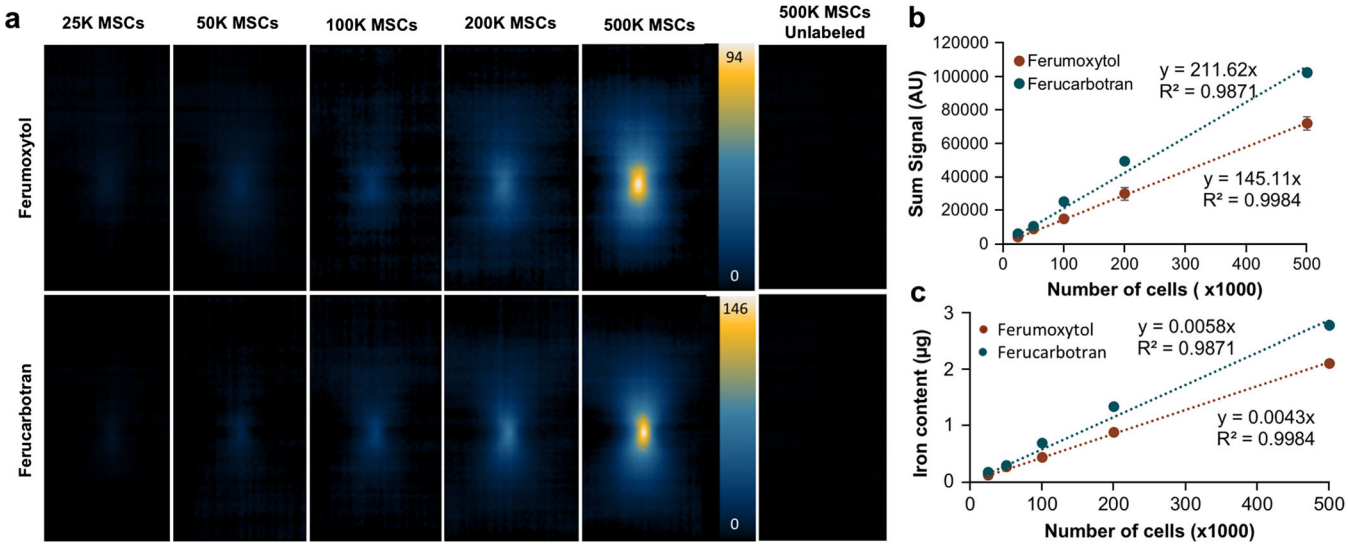

Fig. 3. Magnetic particle images of ferumoxytol- and ferucarbotran-labeled mesenchymal stromal cells (MSCs). **a** MPI images of increasing numbers of ferumoxytol- and ferucarbotran-labeled MSCs in test tubes with 30 µl of agarose scaffold. **b** Corresponding sum MPI signal for increasing numbers of ferumoxytol- and ferucarbotran-labeled MSC. **c** Corresponding total iron content (microgram per cell sample) in increasing numbers of ferumoxytol- and ferucarbotran-labeled MSC, as determined by mass spectrometry.

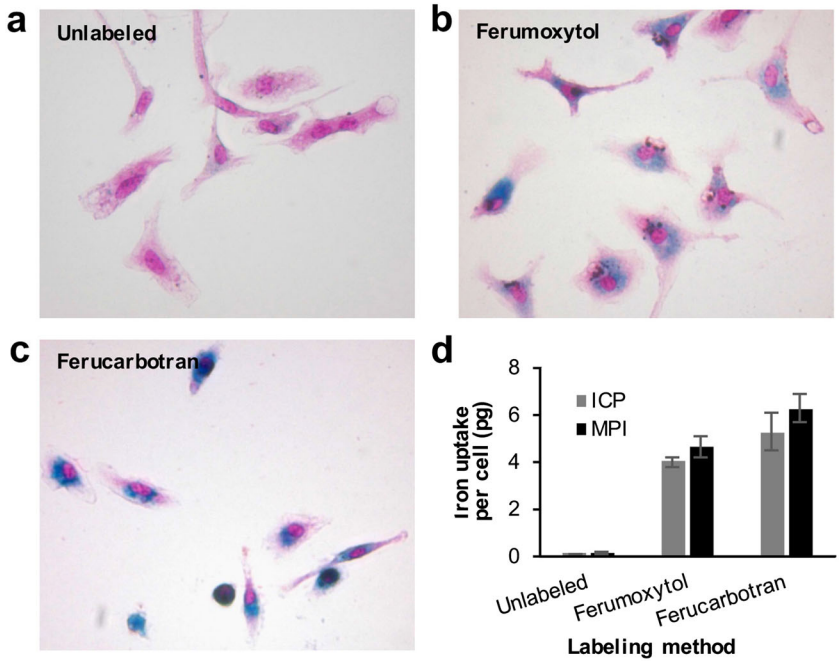

Fig. 4. Cellular iron uptake of ferumoxytol and ferucarbotran. Prussian blue stain of **a** unlabeled MSC, **b** ferumoxytol-labeled MSC and **c** ferucarbotran-labeled MSC. **d** Cellular iron uptake in unlabeled, ferumoxytol, and ferucarbotran-labeled MSCs as measured by ICP and as estimated by MPI. There was no significant difference between iron measures with ICP and iron estimates with MPI ($p = 0.14$).

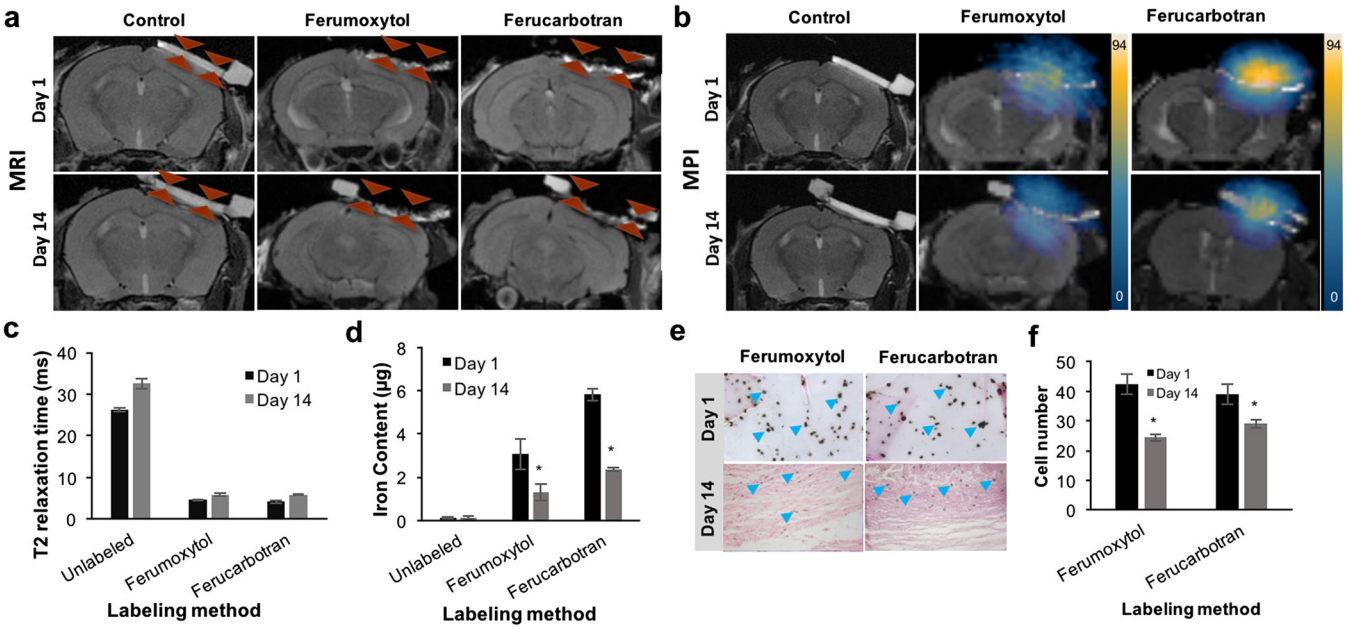

Fig. 5. *In vivo* MRI and MPI of labeled MSC implants in calvarial defects. **a** Coronal fast spin echo (FSE; TE/TR = 42 ms/3000 ms) MR images at day 1 and 14 after implantation of unlabeled, ferumoxytol or ferucarbotran-labeled MSC in calvarial defects of experimental mice. **b** Corresponding MPI images of the same calvarial defects at different time points after implantation of unlabeled, ferumoxytol or ferucarbotran-labeled MSC. **c** Corresponding T2 relaxation times of the calvarial defects at different time points after implantation of unlabeled, ferumoxytol or ferucarbotran-labeled MSC, as measured using multi-echo spin echo (MESE) sequence (TR = 2000 ms, TE = 6, 13, 20, 27, 34, and 41 ms). Data are displayed as means and standard deviations of three animals per experimental group. **d** Corresponding calculated Fe content of the MSC implants at different time points after implantation, as estimated based on their MPI signals. **e** Corresponding DAB-Prussian blue stain and **f** quantification of transplanted MSCs seeded in the scaffold at day 1 and day 14. A single asterisk indicates significant differences between data obtained at day 1 and day 14 ($p < 0.05$).

significantly between day 1 and day 14 for both ferumoxytol- and ferucarbotran-labeled MSC ($p = 0.93$ and $p = 0.23$ respectively).

Discussion

Our results show that ferumoxytol nanoparticles can be used for *in vivo* detection of stem cell transplants. MPI provided information about decreasing ferumoxytol quantities at the transplant site, which was not attainable with MRI.

MPI has several advantages compared to MRI: MPI directly detects the electronic magnetization of iron oxide nanoparticles by applying a time-varying homogeneous excitation field that causes magnetization of the iron oxides to instantaneously flip, and thus induces a signal in the receive coil [28]. The MPI signal is 10^8 times larger than nuclear magnetization of protons seen in MRI, making MPI a sensitive imaging modality for imaging iron. However, it should be noted that being a new and evolving modality, the theoretical detection sensitivity of MPI has not yet been fully realized. MPI directly detects iron oxide nanoparticles, without false positive background signal [29]. Additionally, the nanoparticle signal on MPI increases linearly with increasing nanoparticle concentration, thereby allowing for more accurate iron quantification than MRI [13]. Although, there are no clinical scanners to date, the technology is in principle clinically translatable [30].

Thus far, iron oxide nanoparticle-labeled cells have been tracked with MRI [31]. MRI also allows for quantification of decreasing T2 relaxation times over time [11, 32]. However, changes in T2 and T2* relaxation times are not linearly related to iron concentration or MSC cell number [33], because they are dependent on additional variables, such as intra- or extracellular iron oxide nanoparticle compartmentalization [34], nanoparticle distribution volume, and proton content of the underlying tissue [35].

While we found a linear relationship between MPI signal and iron concentration at a given time point, caution has to be taken with regard to extrapolations of this observation towards changes in cell number over time. The iron content at the transplant site could change due to proliferation of labeled cells, dilution in progenies, iron metabolization, and potential cellular iron elimination. However, assuming differences in cell engraftment and iron metabolization, it would be possible to establish standards for MPI signal over time for successful and unsuccessful cell transplants. Deviations from a reference standard could then be used to diagnose complications of the procedure.

Technical refinements of the sensitivity and image quality of the MPI technique are ongoing, including the design of optimized nanoparticles [36, 37] and pulse sequences with improved sensitivity, such as pulsed excitation waveforms [38, 39]. Hardware improvements, such as incorporating dual-channel, orthogonal drive fields, along with advanced image processing tools that will further improve image quality by achieving isotropic resolution [40, 41] and reducing background image haze [42, 43]. Ultimately, clinical translation of MPI will depend on clinical hardware and clinically applicable nanoparticles. We used lipofectin as a transfection agent to label the cells with ferumoxytol, which is not clinically translatable. There are alternate, transfection agent free options to achieve cell labeling in a clinical setting, such as *in vivo* labeling [44] or utilizing the formation of a protein corona around nanoparticles [17]. Ferumoxytol could be immediately used for cell tracking in a clinical setting [45].

Conclusion

In conclusion, MPI is a new and emerging imaging modality, which can detect iron oxide nanoparticles with high specificity. Our data showed that clinically applicable ferumoxytol nanoparticles can be readily detected with MPI, allowing accurate *in vivo* detection and quantification of ferumoxytol-labeled stem cells. This discovery is an important basis for clinical translation of MPI technologies.

Funding Information. This work was supported by a grant from the Musculoskeletal Transplant Foundation and a grant from the National Institute of Arthritis and Musculoskeletal and Skin Diseases (NIAMS) grant no. 4R01AR054458-09.

Compliance with Ethical Standards

Conflict of Interest

Prachi Pandit holds equity interest in Magnetic Insight Inc.

References

1. Brooks PM (2002) Impact of osteoarthritis on individuals and society: how much disability? Social consequences and health economic implications. Curr Opin Rheumatol 14:573–577
2. Chimutengwende-Gordon M, Khan WS (2012) Advances in the use of stem cells and tissue engineering applications in bone repair. Curr Stem Cell Res Ther 7:122–126
3. Ciapetti G, Granchi D, Baldini N (2012) The combined use of mesenchymal stromal cells and scaffolds for bone repair. Curr Pharm Design 18:1796–1820
4. Jorgensen C, Gordeladze J, Noel D (2004) Tissue engineering through autologous mesenchymal stem cells. Curr Opin Biotechnol 15:406–410
5. Buza JA 3rd, Einhorn T (2016) Bone healing in 2016. Clin Cases Miner Bone Metab 13:101–105
6. Hodgetts SI, Beilharz MW, Scalzo AA, Grounds MD (2000) Why do cultured transplanted myoblasts die in vivo? DNA quantification shows enhanced survival of donor male myoblasts in host mice depleted of CD4+ and CD8+ cells or Nk1.1+ cells. Cell Transplant 9:489–502
7. Rando TA, Pavlath GK, Blau HM (1995) The fate of myoblasts following transplantation into mature muscle. Exp Cell Res 220:383–389
8. Pittenger MF, Martin BJ (2004) Mesenchymal stem cells and their potential as cardiac therapeutics. Circ Res 95:9–20
9. Le Blanc K, Ringden O (2005) Immunobiology of human mesenchymal stem cells and future use in hematopoietic stem cell transplantation. Biol Blood Marrow Trans 11:321–334
10. Koga H, Engebretsen L, Brinchmann JE, Muneta T, Sekiya I (2009) Mesenchymal stem cell-based therapy for cartilage repair: a review. Knee Surg Sports Traumatol Arthrosc 17:1289–1297
11. Hyun J, Grova M, Nejadnik H, Lo D, Morrison S, Montoro D, Chung M, Zimmermann A, Walmsley GG, Lee M, Daldrup-Link H, Wan

DC, Longaker MT (2013) Enhancing in vivo survival of adipose-derived stromal cells through Bcl-2 overexpression using a minicircle vector. Stem Cells Transl Med 2:690–702
12. Bulte JW, Walczak P, Janowski M, Krishnan KM, Arami H, Halkola A, Gleich B, Rahmer J (2015) Quantitative "hot spot" imaging of transplanted stem cells using superparamagnetic tracers and magnetic particle imaging (MPI). Tomography 1:91–97
13. Zheng B, von See MP, Yu E, Gunel B, Lu K, Vazin T, Schaffer DV, Goodwill PW, Conolly SM (2016) Quantitative magnetic particle imaging monitors the transplantation, biodistribution, and clearance of stem cells in vivo. Theranostics 6:291–301
14. Gleich B, Weizenecker J (2005) Tomographic imaging using the nonlinear response of magnetic particles. Nature 435:1214–1217
15. Hope MD, Hope TA, Zhu C, Faraji F, Haraldsson H, Ordovas KG, Saloner D (2015) Vascular imaging with ferumoxytol as a contrast agent. Am J Roentgenol 205:W366–W373
16. Netto JP, Iliff J, Stanimirovic D, Krohn KA, Hamilton B, Varallyay C, Gahramanov S, Daldrup-Link H, d'Esterre C, Zlokovic B, Sair H, Lee Y, Taheri S, Jain R, Panigrahy A, Reich DS, Drewes LR, Castillo M, Neuwelt EA (2018) Neurovascular unit: basic and clinical imaging with emphasis on advantages of ferumoxytol. Neurosurgery 82:770–780
17. Nejadnik H, Taghavi-Garmestani SM, Madsen SJ, Li K, Zanganeh S, Yang P, Mahmoudi M, Daldrup-Link HE (2018) The protein corona around nanoparticles facilitates stem cell labeling for clinical MR imaging. Radiology 286:938–947
18. Song G, Chen M, Zhang Y, Cui L, Qu H, Zheng X, Wintermark M, Liu Z, Rao J (2018) Janus Iron oxides@ semiconducting polymer nanoparticle tracer for cell tracking by magnetic particle imaging. Nano Lett 18:182–189
19. Castaneda RT, Khurana A, Khan R, Daldrup-Link HE (2011) Labeling stem cells with ferumoxytol, an FDA-approved Iron oxide nanoparticle. J Visualized Exp. https://doi.org/10.3791/3482
20. Bullivant JP, Zhao S, Willenberg BJ, Kozissnik B, Batich C, Dobson J (2013) Materials characterization of Feraheme/ferumoxytol and preliminary evaluation of its potential for magnetic fluid hyperthermia. Int J Mol Sci 14:17501–17510
21. Coyne DW (2009) Ferumoxytol for treatment of iron deficiency anemia in patients with chronic kidney disease. Expert Opin Pharmacother 10:2563–2568
22. Bashir MR, Bhatti L, Marin D, Nelson RC (2015) Emerging applications for ferumoxytol as a contrast agent in MRI. J Magn Reson Imaging 41:884–898
23. Nejadnik H, Lenkov O, Gassert F, Fretwell D, Lam I, Daldrup-Link HE (2016) Macrophage phagocytosis alters the MRI signal of ferumoxytol-labeled mesenchymal stromal cells in cartilage defects. Sci Rep 6:25897
24. Wang Y-XJ (2011) Superparamagnetic iron oxide based MRI contrast agents: current status of clinical application. Quant Imaging Med Surg 1:35–40
25. Reimer P, Rummeny EJ, Daldrup HE, Balzer T, Tombach B, Berns T, Peters PE (1995) Clinical results with Resovist: a phase 2 clinical trial. Radiology 195:489–496
26. VivoTrax™ Super-paramagnetic iron oxide tracer for pre-clinical Magnetic Resonance and Magnetic Particle Imaging. https://www.magneticinsight.com/vivotrax/ (accessed 12/20/2017)
27. Ferguson RM, Khandhar AP, Kemp SJ, Arami H, Saritas EU, Croft LR, Konkle J, Goodwill PW, Halkola A, Rahmer J, Borgert J, Conolly SM, Krishnan KM (2015) Magnetic particle imaging with tailored Iron oxide nanoparticle tracers. IEEE Trans Med Imaging 34:1077–1084
28. Goodwill PW, Tamrazian A, Croft LR, Lu CD, Johnson EM, Pidaparthi R, Ferguson RM, Khandhar AP, Krishnan KM, Conolly SM (2011) Ferrohydrodynamic relaxometry for magnetic particle imaging. Appl Phys Lett 98:262502
29. Panagiotopoulos N, Duschka RL, Ahlborg M, Bringout G, Debbeler C, Graeser M, Kaethner C, Lüdtke-Buzug K, Medimagh H, Stelzner J, Buzug TM, Barkhausen J, Vogt FM, Haegele J (2015) Magnetic particle imaging: current developments and future directions. Int J Nanomedicine 10:3097–3114
30. Mason EE, Cooley CZ, Cauley SF et al (2017) Design analysis of an MPI human functional brain scanner. Int J Magn Part Imaging 3. https://doi.org/10.18416/ijmpi.2017.1703008
31. Khurana A, Nejadnik H, Chapelin F, Lenkov O, Gawande R, Lee S, Gupta SN, Aflakian N, Derugin N, Messing S, Lin G, Lue TF, Pisani L, Daldrup-Link HE (2013) Ferumoxytol: a new, clinically applicable label for stem-cell tracking in arthritic joints with MRI. Nanomed 8:1969–1983
32. Daldrup-Link HE, Chan C, Lenkov O, Taghavigarmestani S, Nazekati T, Nejadnik H, Chapelin F, Khurana A, Tong X, Yang F, Pisani L, Longaker M, Gambhir SS (2017) Detection of stem cell transplant rejection with ferumoxytol MR imaging: correlation of MR imaging findings with those at Intravital microscopy. Radiology 284:495–507
33. Nguyen PK, Riegler J, Wu JC (2014) Stem cell imaging: from bench to bedside. Cell Stem Cell 14:431–444
34. Henning TD, Wendland MF, Golovko D, Sutton EJ, Sennino B, Malek F, Bauer JS, McDonald DM, Daldrup-Link H (2009) Relaxation effects of ferucarbotran-labeled mesenchymal stem cells at 1.5T and 3T: discrimination of viable from lysed cells. Magn Reson Med 62:325–332
35. Tromsdorf UI, Bigall NC, Kaul MG, Bruns OT, Nikolic MS, Mollwitz B, Sperling RA, Reimer R, Hohenberg H, Parak WJ, Förster S, Beisiegel U, Adam G, Weller H (2007) Size and surface effects on the MRI Relaxivity of manganese ferrite nanoparticle contrast agents. Nano Lett 7:2422–2427
36. Tay ZW, Hensley DW, Vreeland EC, Zheng B, Conolly SM (2017) The relaxation wall: experimental limits to improving MPI spatial resolution by increasing nanoparticle core size. Biomed Phys Eng Express 3:035003
37. Ferguson RM, Minard KR, Krishnan KM (2009) Optimization of nanoparticle core size for magnetic particle imaging. J Magn Magn Mater 321:1548–1551
38. Goodwill PW, Konkle JJ, Zheng B et al (2012) Projection x-space magnetic particle imaging. IEEE Trans Med Imaging 31:1076–1085
39. Tay ZHD, et al. (2017) Eight fold improvement in magnetic particle imaging resolution with pulsed drive waveform. [Abstract]
40. Zheng B, Yu E, Orendorff R, Lu K, Konkle JJ, Tay ZW, Hensley D, Zhou XY, Chandrasekharan P, Saritas EU, Goodwill PW, Hazle JD, Conolly SM (2017) Seeing SPIOs directly in vivo with magnetic particle imaging. Mol Imaging Biol 19:385–390
41. Lu KGP, Zheng B, Conolly S. (2017) Multi-channel Acquisition for Isotropic Resolution in Magnetic Particle Imaging. [abstract]. 1P
42. Konkle JJ, Goodwill PW, Hensley DW, Orendorff RD, Lustig M, Conolly SM (2015) A convex formulation for magnetic particle imaging x-space reconstruction. PLoS One 10:e0140137
43. Lu KGP, Zheng B, Conolly S (2015) Reshaping the 2D MPI PSF to be isotropic and sharp using vector acquisition and equalization [abstract]. 1P
44. Khurana A, Chapelin F, Beck G, Lenkov OD, Donig J, Nejadnik H, Messing S, Derugin N, Chan RCF, Gaur A, Sennino B, McDonald DM, Kempen PJ, Tikhomirov GA, Rao J, Daldrup-Link HE (2013) Iron administration before stem cell harvest enables MR imaging tracking after transplantation. Radiology 269:186–197
45. Aghighi M, Theruvath AJ, Pareek A, Pisani LL, Alford R, Muehe AM, Sethi TK, Holdsworth SJ, Hazard FK, Gratzinger D, Luna-Fineman S, Advani R, Spunt SL, Daldrup-Link HE (2018) Magnetic resonance imaging of tumor associated macrophages: clinical translation. Clin Cancer Res. https://doi.org/10.1158/1078-0432.CCR-18-0673